Step Instabilities: A New Kinetic Route to 3D Growth

K. M. Chen, D. E. Jesson, S. J. Pennycook, M. Mostoller, and T. Kaplan
Solid State Division, Oak Ridge National Laboratory, Oak Ridge, Tennessee 37831-0631

T. Thundat and R. J. Warmack
Health Sciences Research Division, Oak Ridge National Laboratory, Oak Ridge, Tennessee 37831-6123
(Received 27 December 1994)

Atomic force microscopy studies of Ge/Si(001) molecular beam epitaxy growth reveal a crucial new role of surface steps in the 2D to 3D transition. At or near step flow we show that S_A steps undergo a stress-driven triangular step instability. The resulting spatial variation of surface strain, although small, can dramatically influence the activation barrier for 3D island nucleation. This provides a surprising kinetic route for the onset of 3D growth associated with the apex regions of triangular steps.

PACS numbers: 68.55.Bd, 68.35.–p

Ge deposition on Si(001) by molecular beam epitaxy is a classic example of the Stranski-Krastanow growth mode in which the formation of a two-dimensional (2D) wetting layer is followed by three-dimensional (3D) islanding. Thermodynamically, the 2D to 3D transition is driven by the reduction in strain energy associated with the elastic deformation of the island morphology. However, many of the details of this transition remain unclear, primarily because kinetics can profoundly influence the pathway to islanding during far-from-equilibrium growth [1]. In this Letter we reveal a surprising route to 3D growth at or *near* step flow conditions which involves the stress-driven 2D instability of monolayer height steps. Although the resulting spatial variation of surface stress associated with the step instability is found to be small, it can dramatically affect the activation barrier for 3D island nucleation. This is sufficient to kinetically trigger the nucleation of islands at favored sites, thus defining a crucial new role of surface steps and step instabilities in the 2D to 3D transition.

To investigate the detailed mechanisms governing the 2D to 3D transition, it is necessary to capture the critical stage of growth associated with the formation of 3D islands. This was achieved by depositing 8 monolayers of Ge at 430°C and 0.1 Å s^{-1} on a Si(001) substrate miscut by 0.06° toward [110]. The rather striking and complex morphology occurring during the transition is directly revealed by the atomic force microscopy (AFM) image of the quenched sample shown in Fig. 1. Long wavelength triangular steps, which we nominally refer to as S_A^N steps, can be observed to alternate with relatively straight S_B^N steps which are perpendicular to the dimer rows. This instability is most surprising since it is known that surface steps undergo only random small scale fluctuations during Si homoepitaxy [2]. The pronounced triangular rather than sinuous nature of the instability would appear directly analogous to faceting. Even more surprising, however, is the presence of 2 nm high macroislands at the apex regions of the triangles. This clearly demonstrates that step instability plays a central role in the 2D to 3D transition. We now explain this link by considering the stability of surface steps in the presence of misfit stress and identify the important consequences for 3D island nucleation.

The link between the triangle step instability and surface stress can be established as follows. During the initial stages of step flow growth, we observe that the step instability occurs prior to the nucleation of 3D islands. This demonstrates that the triangular steps are not caused by the pinning of step motion by 3D structures. Furthermore, the $(2 \times N)$ reconstruction of the Ge(001) surface is associated with an anisotropic surface stress tensor. Since the surface steps in Fig. 1 separate alternating $(2 \times N)$ and $(N \times 2)$ surface reconstructions, they also serve as stress domain boundaries. It is known that arrangements of alternating domains are favorable since this can minimize the elastic energy associated with the surface stress [3]. An effective way of enhancing the

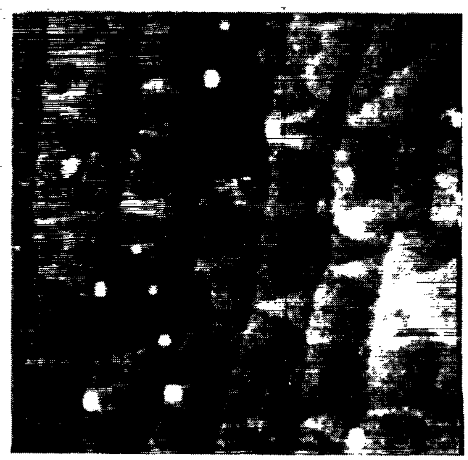

FIG. 1. AFM image of the Ge/Si(001) surface showing a triangular step instability and preferential island nucleation at apex regions. The scan size is 1600×1600 nm^2. Two types of steps can be seen in the image, triangular S_A^N steps and straight S_B^N steps. 3D macroislands appear as bright dots. The spacing (L) between adjacent S_B steps is about 2800 Å, and the average spacing between adjacent triangles of S_A^N steps is 1800 Å.

0031-9007/95/75(8)/1582(4)$06.00

efficiency of this "mixing" process is by transforming a straight step to a wavy step at domain boundaries, which provides a driving force for step instability [4]. In particular, this is consistent with the observed spatial phase relationship between S_A^N steps in Fig. 1. The peak of a triangular S_A^N step generally coincides with the valley of the next closest S_A^N step. This out-of-phase relationship between surface stress domains provides strong evidence for a stress-driven instability of surface steps. We now demonstrate how, in the presence of misfit stress, this step instability can assume dramatic importance even during far-from-equilibrium growth.

To evaluate the elastic energy $E_{\rm el}$ relieved by a triangular step as shown in Figs. 1 and 3, we utilize a surface elastic Green's function approach [3–5] giving

$$E_{\rm el} = -\tfrac{1}{2}\int d\mathbf{x}\, d\mathbf{x}'\, \chi_{ij}(\mathbf{x}-\mathbf{x}') f_i(\mathbf{x}) f_j(\mathbf{x}'), \qquad (1)$$

where $\mathbf{x}$ and $\mathbf{x}'$ are 2D position vectors on the surface. The force density $f_i(\mathbf{x}) = \partial_j \sigma_{ij}(\mathbf{x})$ at position $\mathbf{x}$ produces a displacement $u_i(\mathbf{x}') = \chi_{ij}(\mathbf{x}-\mathbf{x}') f_j(\mathbf{x})$ at $\mathbf{x}'$, where χ is the elastic Green's function of the surface and $\sigma_{ij}(\mathbf{x})$ is the surface stress tensor. The force density is zero, except at the triangular stress domain boundaries, so that the difference in elastic energy per unit area between a wavy triangular step of base λ and height A (as seen in Figs. 1 and 3) and a straight step is given by

$$\Delta E_{\rm el} = -[F_0{}^2(1-\nu)/\pi\mu L][E(\lambda,A) - \ln(L/2\pi a)]. \qquad (2)$$

Here μ is the shear modulus and ν Poisson's ratio; L is the spacing between adjacent S_B^N straight steps and a is the surface lattice constant. If $\sigma_\parallel$ and $\sigma_\perp$ define the respective components of the surface stress tensor parallel and perpendicular to the dimer rows, then the stress anisotropy is characterized by $F_0 = \sigma_\parallel - \sigma_\perp$. The quantity $E(\lambda, A)$ reflects the contribution of the triangular step waviness to the elastic energy and is conveniently evaluated numerically as a reciprocal space summation.

The reduction in elastic energy due to step waviness [Eq. (2)] is offset by the creation of additional step energy per unit area $\Delta E_{\rm st}$. In particular, the waviness of an S_B^N (S_A^N) step requires the creation of kinks involving S_A (S_B) steps of energy $\varepsilon_{A(B)}$ per unit length, giving

$$\Delta E_{\rm st} = 2\varepsilon A/\lambda L. \qquad (3)$$

The additional energy associated with a kink is $\varepsilon = \varepsilon_{A(B)} + n\varepsilon_C - \varepsilon_e(T)$, where n is the number of corners per unit length of step edge, with energy ε_C per corner, and $\varepsilon_e(T)$ is the temperature dependent entropic contribution [6] to step-free energy per unit length. The triangular nature of the step instability in our images can be understood in terms of kink-kink interactions in a manner entirely analogous to 3D faceting, and these effects could be incorporated approximately by suitably modifying the corner energy ε_C. The triangular step waviness contribution to the surface energy is therefore

$$\Delta E = \Delta E_{\rm el} + \Delta E_{\rm st} = -[F_0{}^2(1-\nu/\pi\mu L][E(\lambda,A) - \ln(L/2\pi a)] + (2A/\lambda L)\varepsilon. \qquad (4)$$

Equation (4) is our principal result defining the stability of surface steps. Consider first the case of zero misfit. For the Si(001) surface, F_0 has been calculated [7] to be 0.26 eV Å^{-2}, and from Ref. [8] we estimate ε to be 8 meV Å^{-1} for the S_A kink segment of S_B^N steps and 23 meV Å^{-1} for S_B kink segments of the S_A^N steps at 430°C. Inserting these values into Eq. (4), we plot ΔE as a function of instability amplitude in Fig. 2. For a representative wavelength of 1800 Å, we find S_A^N steps to be stable, while the activation barrier of 5.4 eV for S_B^N steps is considerably greater than the available thermal energy of 60 meV. We find a similar behavior for all wavelengths. This demonstrates that instabilities due to surface stress are kinetically suppressed for both steps at low temperatures. At higher temperatures the free energies of S_A and S_B steps reduce due to the increasing entropic contribution, vanishing at about 1230°C [9]. As revealed in Fig. 2, the step instability is therefore barrierless at high temperatures consistent with the sinuous S_A^N and S_B^N step geometries observed by Tromp and Reuter [10].

We now evaluate ΔE for Ge/Si(001) at 430°C. To evaluate the surface stress anisotropy F_0 and the kink en-

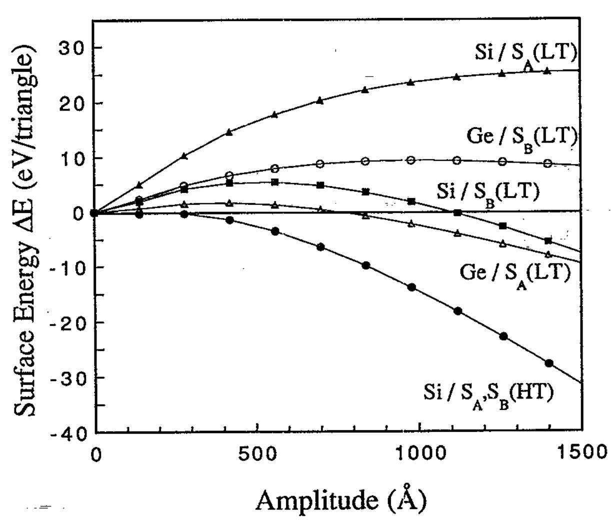

FIG. 2. Contribution of the step waviness to surface energy (ΔE) per triangle as a function of amplitude (A) for S_A^N and S_B^N steps on Si(001) and Ge(001) surfaces at various temperatures. For a wavelength of 1800 Å and a terrace width of 2800 Å, both steps are unstable at high temperature (1230°C denoted by HT). At low temperature (430°C denoted by LT), a significant activation barrier suppresses step waviness on Si(001), while on the strained Ge film the barrier for S_A^N steps is greatly reduced. Similar behavior is observed for all wavelenghts.

ergy ε, we have employed classical potential molecular dynamics calculations using the Stillinger-Weber potential [11–13]. The surface stress tensor is rather sensitive to the $(2 \times N)$ reconstruction of the Ge surface, although for N = 8, as observed by reflection high-energy electron diffraction (RHEED) during deposition, we find a stress anisotropy $F_0 = 0.20$ eV Å^{-2}, similar to that of Si(001). Additionally, our calculations reveal that the S_B step or the associated kink energy of a fully strained Ge(001) surface is reduced by 20 meV Å^{-1} compared with the same step and kink geometries on Si(001). In contrast, we find that the S_A step (or associated kink) is virtually unchanged, in agreement with other recent studies [14,15]. Utilizing the experimentally measured step energy values of 8 and 23 meV Å^{-1} for S_A and S_B steps on Si(001), our calculated difference in step energies gives $\varepsilon = 3$ meV Å^{-1} for S_B kink segments of S_A^N steps and $\varepsilon = 8$ meV Å^{-1} for S_A kink segments of S_B^N steps on Ge(001). These changes in step energy can dramatically influence step instability via Eq. (4) as shown by the plots in Fig. 2. Clearly, the instability associated with S_B^N steps is kinetically suppressed at the growth temperature of 430°C. However, the activation barrier for the S_A^N step is only 0.5 eV per triangle, which is comparable to the thermal energy. This explains why the S_A^N step is unstable to triangular undulations in Fig. 1, whereas the S_B^N step is straight. Therefore, even during far-from-equilibrium growth, misfit stress can destabilize surface steps. This must inevitably modify the spatial distribution of surface stress, and we now consider the important implications for the onset of 3D growth.

The spatial variation of the strain field $\Delta\varepsilon_{ij} = \frac{1}{2}[(\partial d_i/\partial x_j) + (\partial d_j/\partial x_i)]$ associated with the step instability can be evaluated from our Green's function analysis of the total integrated displacement field **d**. $\Delta\varepsilon_{xx}$ has the most rapid spatial variation while $\Delta\varepsilon_{yy}$ is smaller by a factor of 10 with a slower spatial variation and the shear components $\Delta\varepsilon_{xy}$ are zero. The $\Delta\varepsilon_{xx}$ component is displayed in Fig. 3. Apex regions (P) possess the greatest compressive strains, whereas the triangle intersections (I) are most relaxed. This strain variation results in a maximum strain energy difference of 3 meV per adatom, which is considerably smaller than the thermal energy. The spatial variation of the adatom density due to the surface strain fluctuations is therefore negligible. However, as discussed earlier, such stresses are large enough to influence the spatial "phase" relationship between stress domains in Fig. 1. In particular, we find a pronounced tendency for an out-of-phase condition such that the peaks of a triangular S_A^N step are close to the valleys of the next closest S_A^N step. Compared with the in-phase condition, this ensures a more efficient reduction in long-range surface stresses.

Now consider the growth of a pyramidal island on a surface region associated with local stress σ_{xx}, σ_{yy}. If we assume that the spatial variation of this stress is slow compared with the dimensions of the island, and since

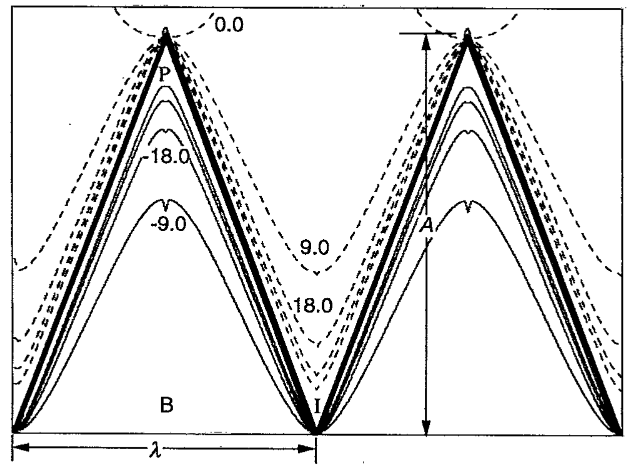

FIG. 3. Spatial variations of surface strain $\Delta\varepsilon_{xx}$, resulting from the interaction of stress domains with $A = 2800$ Å and $\lambda = 2000$ Å. Solid contours indicate compressive contributions ($\times 10^{-4}$) which add to the initial misfit strain and cause the apex of each triangle (P) to be the most strained regions of the film surface. Dotted contours indicate regions which relax the initial misfit stress, the least strained regions (I) occurring at the valleys. The base of triangle (B) is close to the initial misfit strain.

$\sigma_{xx} \approx \sigma_{yy}$, the minimum energy island shape is a square-based pyramid, then the island energy is given by [16]

$$E = 4\Gamma V^{2/3} \tan^{1/3}\theta - 3(c_1 + c_2) V \tan\theta . \quad (5)$$

Here θ is the inclination of the pyramid faces to the substrate, $\Gamma = \gamma_e csc\theta - \gamma_s \cot\theta$ where γ_s and γ_e are respective free energy per unit area for the planar surface and the beveled facet and $c_1 = \sigma_{xx}^2(1 - \nu)/2\pi\mu$, $c_2 = \sigma_{yy}^2(1 - \nu)/2\pi\mu$. In Fig. 4 we plot this energy as a function of island volume V [17]. The plots demonstrate that an activation barrier (E_a) exists for the onset of 3D growth. This is associated with the formation of a critical island nucleus beyond which 3D growth is energetically favorable. The activation barrier and critical island size are sensitive functions of local surface stress, being proportional to $(\sigma_{xx}^2 + \sigma_{yy}^2)^{-2}$ and $(\sigma_{xx}^2 + \sigma_{yy}^2)^{-3}$, respectively [16]. As shown in Fig. 4, apex regions (P) with enhanced compressive strain can therefore dramatically reduce the activation barrier. The barrier is calculated to be 2.4 eV for regions far from a step, while in region P (close to the apex of the triangle) the barrier is reduced to only 1.92 eV. The island nucleation rate at apex regions is therefore enhanced by a factor of $\exp(\Delta E_a/kT) \sim 3 \times 10^3$. Although this estimate is necessarily qualitative in nature due to uncertainties in surface energies, it is in excellent agreement with our experimental observations. We have measured the spatial distribution of 3D islands over large regions to determine the statistical significance of preferred nucleation sites. Approximately half of the total number of 3D islands are

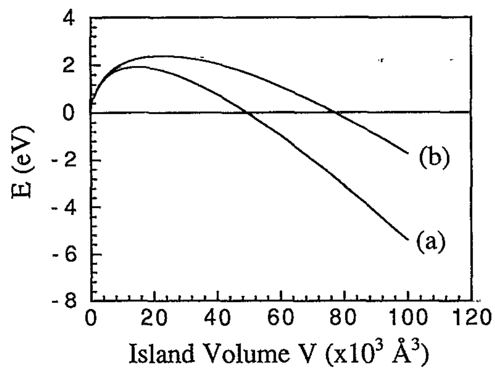

FIG. 4. Island energy E versus island volume V at (a) the highly strained apex region and (b) the base of the triangle. The excess surface strain at the apex region significantly reduces the activation barrier and critical nucleus size, explaining the preferential nucleation observed in Fig. 1.

located at or close to apex regions, 30% are located at or near step edges but away from the apex regions, and the remaining 20% are located on terraces away from step edges. Estimating the area of apex and step edge regions to be 0.1% and 1% of the total surface area, respectively, then the experimentally observed nucleation rate at the apex regions is enhanced by a factor of 2500 compared with the terrace nucleation rate. This is in good agreement with our theoretical estimate of 3000. Similarly, the increased nucleation rate close to the step edge is consistent with regions of enhanced stress relative to the terrace (Fig. 3), where the energy barrier is estimated to be 2.1 eV.

Based on our observations and calculations, we can now establish the route of the 2D to 3D transition at or near step flow conditions. The first three monolayers of Ge deposition occur in a 2D mode during which, type S_A^N steps are unstable to the formation of triangular stress domains. Following the deposition of this wetting layer, a driving force exists to form 3D islands. However, this is kinetically suppressed by the activation barrier for 3D island nucleation. The spatial variation in surface stress provides preferential nucleation sites at the apex regions of triangles which locally reduce the activation barrier and critical nucleus size for 3D island formation. This is sufficient to kinetically trigger the onset of 3D growth. On the terraces the activation barrier for 3D island nucleation is large, which is supported by the presence of 2 to 4 monolayer high unstable clusters as seen in high magnification AFM images [18].

The rather surprising implication of this study is that stress domains separated by monolayer height steps can dramatically influence the growth mode in the presence of misfit stress. This conceivably has quite general ramifications for the growth of strained layers and alloy systems where spatial variations in surface stress might lead to elemental clustering. This could explain the interesting phenomenon of Ge clustering in SiGe alloy superlattices which is thought to be responsible for enhanced luminescence peaks [19].

This research was sponsored by the Division of Material Science, U.S. Department of Energy under Contract No. DE-AC05-84OR21400 with Martin Marietta Energy System, Inc., and in part by an appointment to the Oak Ridge National Laboratory Postdoctoral Research Program administrated by Oak Ridge Institute for Science and Education.

[1] Y.-W. Mo, D.E. Savage, B.S. Swartzentruber, and M.G. Lagally, Phys. Rev. Lett. **65**, 1020 (1990).
[2] See, for example, Y.-W. Mo *et al.*, J. Vac. Sci. Technol. A **8**, 201 (1990).
[3] O.A. Alerhand, D. Vanderbilt, R.D. Meade, and J.D. Joannopoulos, Phys. Rev. Lett. **61**, 1973 (1988).
[4] J. Tersoff and E. Pehlke, Phys. Rev. Lett. **68**, 816 (1992).
[5] L.D. Landau and E.M. Lifshitz, *Theory of Elasticity* (Pergamon, New York, 1970).
[6] O.L. Alerhand *et al.*, Phys. Rev. Lett. **64**, 2406 (1990).
[7] M.C. Payne, N. Roberts, R.T. Needs, M. Needels, and J.D. Joannopoulos, Surf. Sci. **211/212**, 1 (1989).
[8] B.S. Swartzentruber, Y.-W. Mo, R. Kariotis, M.G. Lagally, and M.B. Webb, Phys. Rev. Lett. **65**, 1913 (1990).
[9] N.C. Bartelt, R.M. Tromp, and E.D. Williams, Phys. Rev. Lett. **73**, 1656 (1994).
[10] R.M. Tromp and M.C. Reuter, Phys. Rev. Lett. **68**, 820 (1992).
[11] F. Stillinger and T. Weber, Phys. Rev. B **31**, 5262 (1985).
[12] K. Ding and H.C. Andersen, Phys. Rev. B **34**, 6987 (1986).
[13] M. Karimi, T. Kaplan, M. Mostoller, and D.E. Jesson, Phys. Rev. B **47**, 9931 (1993).
[14] Y.H. Xie *et al.*, Phys. Rev. Lett. **73**, 3006 (1994).
[15] F. Wu, X. Chen, Z. Zhang, and M.G. Lagally, Phys. Rev. Lett. **74**, 574 (1995).
[16] J. Tersoff and F.K. LeGoues, Phys. Rev. Lett. **72**, 3570 (1994).
[17] The facet angle θ for the critical nucleus is approximated to be 5°, based on our recent experimental studies of 3D island nucleation. Since there is no available data on the Ge(001) surface energy anisotropy in the literature, we base our estimates on the Si surface energy as given by D.J. Eaglesham, A.E. White, L.C. Feldman, N. Moriya, and D.C. Jacobson, Phys. Rev. Lett. **70**, 1643 (1993). For Si, $\gamma_s = 85$ meV Å^{-2} and $\gamma_e = 85.2$ meV Å^{-2}. We scale these relative values for Ge in proportion to the cohesive energy, i.e., $\gamma_s = 68$ meV Å^{-2} and $\gamma_e = 68.16$ meV Å^{-2}
[18] Similar clusters have been observed by M. Krishnamurthy, J.S. Drucker, and J.A. Venables, J. Appl. Phys. **69**, 6461 (1991).
[19] J.-P. Noel *et al.*, Appl. Phys. Lett. **61**, 690 (1992).